

Synthesis, characterization and cycling performance of novel chromium oxide cathode materials for lithium batteries

Ramaraja P. Ramasamy, P. Ramadass, Bala S. Haran, Branko N. Popov*

Department of Chemical Engineering, Center for Electrochemical Engineering, University of South Carolina, Columbia, SC 29208, USA

Received 15 April 2003; accepted 10 May 2003

Abstract

Chromium oxide (CrO_x) cathode material (with chromium oxidation state of +5.3) was synthesized by thermal decomposition of chromium trioxide at high temperature and pressure in oxygen atmosphere. The duration of thermal decomposition had a significant effect on the performance of these materials in terms of lithiation capacity. The detrimental effect of CrO_3 and lower oxidation state chromium oxides have been reduced considerably by reducing their amounts in the material. The operating conditions, namely, temperature, pressure and the reaction time were optimized based on synthesizing novel CrO_x cathode material with superior properties, such as low irreversible capacity loss, stable capacity and low capacity fade under continuous cycling. These materials are stable intercalation hosts for lithium and were found to be reversible in the entire intercalation range (2.0–4.2 V versus Li/Li^+). The average voltage of these cells is 3 V versus Li/Li^+ . CrO_x -B cathodes exhibit higher capacity than any of the prominent cathode materials used for lithium batteries with an initial lithiation capacity of capacity of 322 mAh/g. The material shows very low capacity fade during cycling and retained 93% of its reversible capacity after 100 cycles.

© 2003 Elsevier B.V. All rights reserved.

Keywords: Lithium batteries; Chromium oxide; Cathode material

1. Introduction

Chromium oxides as cathode materials have attracted attention for rechargeable lithium batteries because of their high energy density and high capacity at low discharge rates [1]. In 1984, the Varta battery company developed cylindrical type Li/CrO_x batteries with energy density of about 800–1000 mWh/cm³ with a nominal voltage of 3 V [2]. Toyoguchi et al. [3] developed a coin type LiCr_2O_5 secondary battery with energy density of 170 Wh/l and a cycle life over 400 cycles. Primary Li/AgCrO_4 cells, utilizing organic electrolytes are manufactured by SAFT [4]. Varta also have developed a primary Li/CrO_x cell with an energy density of 675 Wh/l at low drain rates [4]. Schwartz et al. [5] observed that mixtures of Cr_3O_8 , Cr_2O_5 and CrO_2 are formed in the temperature range of 267–348 °C. It was found that CrO_x , which has a stoichiometry close to that of Cr_3O_8 , exhibits good performance as a reversible cycling material for lithium intercalation and deintercalation reaction [5]. The reversibility for lithium intercalation of the

chromium oxides decreases in the order: $\text{Cr}_3\text{O}_8 > \text{Cr}_2\text{O}_5 > \text{CrO}_2$. Research by Besenhard et al. [6] reported a new type of chromium oxide, $\text{CrO}_x(\text{SO}_3)$, that had better performance even at high rates. Unreacted CrO_3 contamination is comparatively lower in $\text{CrO}_x(\text{SO}_3)$ than in normal CrO_x . Prolonged decomposition of CrO_3 at normal pressure or decomposition at high temperatures and pressures can decrease the contamination by unreacted CrO_3 in the product [6]. A detailed study of the phase compositions at different temperatures showed that Cr_3O_8 was the most suitable material for lithium battery cathodes. High energy density and good rechargeability made it the best material for cathodes for lithium batteries [7]. Amorphous chromium oxides were believed to possess high energy density due to their high specific surface area. Amorphous chromium oxides can be formed by heating CrO_3 with a small amount of water at a suitable temperature and pressure. Theoretically, Cr_3O_8 can transfer 2.3 electrons per atom of Cr [8]. But the batteries developed by Varta [2] accepted an average of 1.4–1.5 electrons for each atom of chromium during their discharge. Koksang et al. [9] noticed that at room temperature both Cr_8O_{21} and Cr_3O_8 are insensitive to overdischarge and these materials can be cycled even at voltages below 2 V. For Cr_3O_8 , an additional 0.4 Li/Cr capacity is obtained when

* Corresponding author. Tel.: +1-803-777-7314; fax: +1-803-777-8265.
E-mail address: popov@engr.sc.edu (B.N. Popov).

discharged at up to 1.8 V [10]. Reports by the same author also say that at elevated temperatures, the number of lithium atoms inserted per formula atom of chromium exceeds four. Detailed studies of chromium oxide cathode materials were done by Arora et al. [11]. They reported a capacity of 255 and 215 mAh/g for CrO_x and LiCrO_x , respectively, during the first discharge with an energy density of approximately 650 Wh/kg. Attempts have been made to improve the performance of chromium oxides by doping with cobalt, which will enable them to perform well at higher discharge rates [12]. $\text{CrO}_{2.5}$ -doped LiMn_2O_4 can also be found in the literature [13]. Crystalline CrO_x can be obtained by heating CrO_3 in an autoclave for 24 h at 500 psi and 270 °C. The formation of CrO_x is highly dependent upon temperature and pressure. Even a slight deviation in the operating parameters will lead to the formation of an oxide of different stoichiometry [14].

The objective of this work is to synthesize a new CrO_x material, which has a very high reversible capacity and low amounts of unreacted CrO_3 . It is believed that the unreacted CrO_3 in the active material synthesized by Arora et al. [11], is the main cause of the large irreversible capacity loss between the first and the second cycles. Moreover, the chromium oxide synthesized by Arora et al. [11], exhibited more capacity fade during cycling. Hence, another objective of this study is the preparation of a material with better reversibility and a lower capacity fade than the cathode materials synthesized by Arora et al. [11].

2. Experimental

Chromium oxide material (CrO_x) having a high oxidation state was obtained by thermal decomposition of chromium trioxide CrO_3 (99.5% pure, Alfa Aesar) along with ammonium sulfate (99% pure, Aldrich) in a ratio of 95:5 at a temperature of 270–290 °C under high oxygen pressure of around 500 psi in an autoclave. The time durations for this decomposition reaction were chosen to be 24, 48, 72 and 96 h. The corresponding cathode samples obtained as a result of decomposition were named as CrO_x -A, CrO_x -B, CrO_x -C and CrO_x -D, respectively. The samples obtained in this method were similar to the m- CrO_x as reported by Arora et al. [11] with little variation in the composition and the duration of thermal decomposition. The product obtained was a mixture of CrO_x and unreacted CrO_3 .

Once the reaction was complete, the autoclave was taken out of the heater and then quenched in ice-cold water. This is done in order to obtain a crystalline product. The product was then ground to fine powder and subjected to purification. Purification was done by leaching the product 10 times with triply distilled de-ionized water and with acetonitrile (99.5% pure, Aldrich) in a vacuum suction filter using Fisher-P8 filter paper. By this method, the traces of unreacted CrO_3 could be removed to a large extent. The purified samples were then dried in vacuum (Yamato ADP-21 oven) at 120 °C for 12 h to remove traces of water. The dried active

material was then ground to a fine powder and then sieved through 100 μm sieves. For making disc electrodes, the active material was mixed with 10% carbon black (Alfa Aesar, conducting additive, 99.9% pure, 80 m^2/g) and 5% PTFE (binder) and then pressed into a thin film of about 50–60 μm thickness. Pellets of 1 cm diameter and about 15 mg weight were prepared for all electrochemical studies.

Electrochemical characterization was done in Cole–Parmer three-electrode cell assembly (T-cells). The counter and the reference electrodes used were disks of pure lithium foil (FMC Corp.) with the newly prepared material as the working electrode. The separator was a sheet of Celgard 2340 microporous separator. The electrolyte used in this study was 1 M LiPF_6 in a 1:1 mixture of EC and DMC. The entire cell assembly was carried out in a glove box filled with dry argon and once the cells were assembled, they were left in the dry box for about 1 h, to ensure the diffusion of the electrolyte into the porous structure of the cathode.

The galvanostatic charge–discharge cycling was carried out using Arbin BT-2043 cycler. Charge–discharge curves were obtained for different current rates for a voltage range of 2.0–4.2 V. Electrochemical impedance spectroscopy (EIS) experiments were carried out at different states of charge using a Solartron-1255 frequency response analyzer between frequency limits of 10 mHz to 10 kHz, with an ac voltage signal of ± 5 mV, which ensured the electrode system to be under minimum perturbation. Z-View software (Scribner Associates Inc.) was used to analyze the impedance data by an equivalent circuit fitting method. X-ray diffraction (XRD) studies were carried out using a Rigaku 405S5 diffractometer with $\text{Cu K}\alpha$ radiation for both powder samples and the pellet electrodes, and the data were analyzed using the JADE software.

3. Results and discussion

3.1. Choice of cathode material

X-ray diffraction analysis of the four different samples, namely, CrO_x -A, CrO_x -B, CrO_x -C and CrO_x -D are shown in Fig. 1. The XRD patterns confirm the crystalline nature of these chromium oxide samples. The presence of impurities and other undesirable oxide materials were identified based on the peak intensities and appearance of new peaks. Identification of impurity oxides helps in the preparation of a better reversible cathode material. XRD patterns of all the oxide samples shows a strong peak around $2\theta = 27^\circ$ which corresponds to the desired oxide material, namely, Cr_3O_8 . The patterns also confirm the presence of some unreacted CrO_3 ($2\theta = 25^\circ$) that indicates either an insufficient purification or that a small portion of the oxide materials remains inert to the leaching solvents, namely, water and acetonitrile. The peak intensity of unreacted CrO_3 was found to decrease as the decomposition time increases. The undesirable oxide material found in the XRD patterns was CrO_2 at $2\theta = 28$,

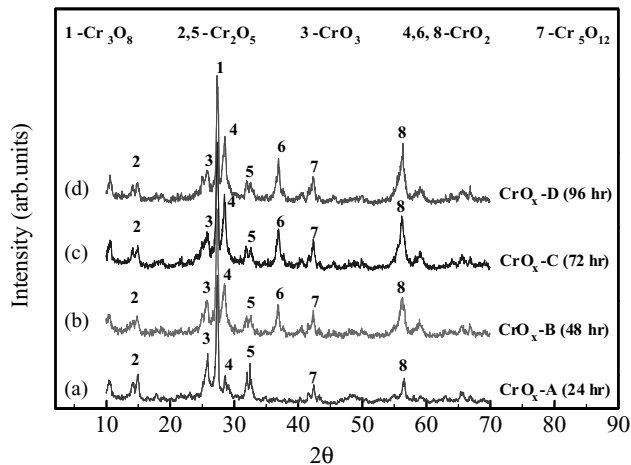


Fig. 1. The powder XRD patterns for different chromium oxides: (a) $\text{CrO}_x\text{-A}$ (24 h); (b) $\text{CrO}_x\text{-B}$ (48 h); (c) $\text{CrO}_x\text{-C}$ (72 h); (d) $\text{CrO}_x\text{-D}$ (96 h).

37 and 56°, whose peak intensities kept increasing with increase in the thermal decomposition time. Peaks at 15 and 32° correspond to Cr_2O_5 , whereas the peak at 43° corresponds to Cr_5O_{12} . Both Cr_2O_5 and Cr_5O_{12} were impurity oxides that do not participate in any useful electrochemical lithium intercalation.

The term undesirable or impure oxide refers to chromium oxides of lower oxidation states, which are produced during prolonged decomposition of CrO_3 . These impure oxide materials have poor reversibility and very low energy density [7]. At the experimental temperature and pressure, the synthesized material is Cr_3O_8 , which has 2.65 atoms of oxygen for each atom of chromium and has been observed to be a good reversible material for lithium intercalation [14].

Fig. 2 shows the first cycle galvanostatic discharge characteristics of all the four samples. The $\text{CrO}_x\text{-B}$ sample shows the best discharge performance. It gives a lithiation capac-

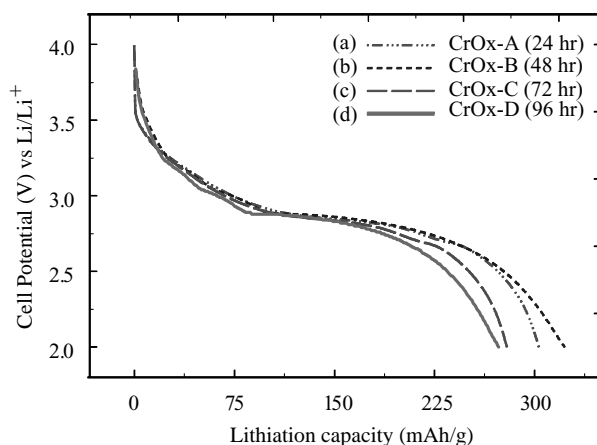


Fig. 2. First discharge curves of different chromium oxides at discharge rate of 0.5 mA/cm^2 : (a) $\text{CrO}_x\text{-A}$ (24 h); (b) $\text{CrO}_x\text{-B}$ (48 h); (c) $\text{CrO}_x\text{-C}$ (72 h); (d) $\text{CrO}_x\text{-D}$ (96 h).

Table 1

Comparison of the first discharge capacities and percentage capacity loss for different chromium oxides

Oxide type	Initial capacity (mAh/g)	Capacity loss (%)	
		Two cycles	Five cycles
$\text{CrO}_x\text{-B}$	322.35	19.485	19.882
$\text{CrO}_x\text{-A}$	303.23	22.941	25.061
$\text{CrO}_x\text{-C}$	279.21	21.045	28.721
$\text{CrO}_x\text{-D}$	273.13	20.598	29.334

ity of 322 mAh/g when cycled at a rate of 0.5 mA/cm^2 ($\sim C/6$ rate). The lithiation capacities of the other samples were found out to be 303, 279 and 273 mAh/g for $\text{CrO}_x\text{-A}$, $\text{CrO}_x\text{-C}$ and $\text{CrO}_x\text{-D}$, respectively, when cycled at the same rate ($C/6$). All oxide samples possess a flat voltage plateau around 3 V during discharge. The cut-off region (2–2.5 V) was comparatively less steep for the $\text{CrO}_x\text{-B}$ when compared with other oxide samples. An additional 20% capacity can be obtained in the range 1.5–2.0 V for these oxides [8,10]. The lithiation capacities for $\text{CrO}_x\text{-A}$, $\text{CrO}_x\text{-B}$, $\text{CrO}_x\text{-C}$ and $\text{CrO}_x\text{-D}$ obtained in this range are 53, 60, 52 and 49 mAh/g, respectively.

Table 1 gives the percentage capacity losses after two and five cycles of galvanostatic charge–discharge for the four samples. All the CrO_x samples have higher irreversible capacity loss between the first and the second discharge steps. While the $\text{CrO}_x\text{-B}$ sample did not show any significant reduction in the capacity after the second cycle, all other oxides invariably showed a continuous reduction in their discharge capacities as is evident from the percentage capacity loss after five cycles. After five cycles, the discharge capacity of the $\text{CrO}_x\text{-B}$ sample is 31.02 mAh/g higher than the $\text{CrO}_x\text{-A}$ sample, and 59.24 and 65.25 mAh/g higher than $\text{CrO}_x\text{-C}$ and $\text{CrO}_x\text{-D}$ samples, respectively. Thus, based on the initial XRD analysis and reversibility behavior, thermal decomposition of CrO_3 at 270 °C and 500 psi for 48 h ($\text{CrO}_x\text{-B}$) was identified to be optimum with regard to maximum conversion of CrO_3 to CrO_x and reducing amount of impurity oxides. $\text{CrO}_x\text{-A}$ sample prepared by thermal decomposition of CrO_3 at 270 °C and 500 psi for 24 h which is similar to the m- CrO_x reported by Arora et al. [11] has been chosen for comparing cycle performance against $\text{CrO}_x\text{-B}$.

3.2. Effect of leaching agent and dispersant

The m- CrO_x was reported as chemically modified with a small amount of $(\text{NH}_4)_2\text{SO}_4$ in it [11]. Ammonium sulfate acts as a dispersant and increases the active area for lithium intercalation. Attempts have been made in this study to see the effect of the dispersant in improving the capacity of the $\text{CrO}_x\text{-B}$ sample. Two different compositions of $\text{CrO}_x\text{-B}$ (2% $(\text{NH}_4)_2\text{SO}_4$ + 98% CrO_3 and 5% $(\text{NH}_4)_2\text{SO}_4$ + 95% CrO_3) were prepared. The T-cells fabricated from these samples were subjected to galvanostatic charge–discharge cycling. The initial and reversible capacities of these two different

Table 2

Effect of leaching solvent and amount of dispersant doping on the capacity and irreversible loss of $\text{CrO}_x\text{-B}$

Dispersant doping	Leaching solvent	Initial capacity (mAh/g)	Reversible capacity (mAh/g)	Irreversible loss (%) ^a
2% $(\text{NH}_4)_2\text{SO}_4$	Acetonitrile	318.37	214.47	32.635
2% $(\text{NH}_4)_2\text{SO}_4$	Water and acetonitrile	320.89	254.45	20.705
5% $(\text{NH}_4)_2\text{SO}_4$	Acetonitrile	320.52	220.74	31.131
5% $(\text{NH}_4)_2\text{SO}_4$	Water and acetonitrile	322.35	259.54	19.485

^a Irreversible loss (%) = [(initial capacity – reversible capacity)/initial capacity] × 100.

samples of $\text{CrO}_x\text{-B}$ were compared in order to determine the effect of the dispersant added. Experiments were also done to study the effect of leaching solvent (water and acetonitrile) over the performance of $\text{CrO}_x\text{-B}$. Two modes of leaching were adopted, namely, leaching with only acetonitrile and leaching with de-ionized water followed by leaching with acetonitrile. Use of de-ionized water as a leaching solvent proved very effective since water has the capability to wash out most of the unreacted CrO_3 , which in effect will reduce the amount of impurities and undesirable oxides in the cathode material and hence can reduce the irreversible capacity loss. The effects of type of leaching solvent and the amount of dispersant are shown in Table 2. The use of de-ionized water as leaching agent along with acetonitrile improves the performance of these materials by reducing the irreversible capacity loss up to 12% when compared with the loss obtained by using acetonitrile alone. On using the same leaching agent, the performance of the oxides does not vary much with the amount of dispersant. As seen from Table 2, if acetonitrile alone is used as leaching agent, the oxides loses 32.6% of its capacity with 2% $(\text{NH}_4)_2\text{SO}_4$ and 31.1% with 5% $(\text{NH}_4)_2\text{SO}_4$. But with the choice of de-ionized water and acetonitrile as leaching agents, the irreversible capacity losses were only 20.7 and 19.4% for oxide samples containing 2 and 5% $(\text{NH}_4)_2\text{SO}_4$, respectively. Hence, increasing the content of $(\text{NH}_4)_2\text{SO}_4$ above 2% does not alter the performance of the CrO_x very much. It is more important to know that thermal decomposition of CrO_3 without the addition of dispersant results in less active surface area and hence it is essential to add at least 2% $(\text{NH}_4)_2\text{SO}_4$ while decomposing CrO_3 in the autoclave. Based on these results, $\text{CrO}_x\text{-B}$ prepared with 5% $(\text{NH}_4)_2\text{SO}_4$, which was leached with water and then purified using acetonitrile was identified as the best material based on the high initial and reversible capacities, low irreversible capacity loss and less undesirable oxide impurities. Hence, $\text{CrO}_x\text{-B}$ was chosen for cycling studies. The samples whose galvanostatic discharge plots are shown in Fig. 2 were leached with both water and acetonitrile with 5% $(\text{NH}_4)_2\text{SO}_4$ in it.

3.3. Analysis of irreversible capacity loss

The irreversible capacity loss is primarily due to the presence of lower oxidation state chromium oxides as most of them are not reversible. The presence of unreacted CrO_3 also accounts for the irreversible loss of capacity. The chromium

trioxide and the impurity oxides undergo irreversible reduction reaction during the first discharge step and decrease the amount of material available for intercalation. Moreover, formation of SEI layer over the surface of the cathode material during the course of lithiation also contributes to the irreversible capacity fade as a result of primary active material loss (Li^+) to form the passive film. The impurities that are not reversible undergo reduction during the first discharge and remain inert. Another possible reason for the reduction in the capacity is that the active lithium may be lost if it forms a composite with the CrO_x , thereby the extraction of all lithium (which intercalates during the first discharge) is not accomplished by recharge to 4.2 V versus Li/Li^+ . Detailed studies of the mechanism leading to irreversible capacity loss in Li-ion batteries can be found elsewhere [15]. A reasonable explanation for the irreversible capacity loss based on the XRD analysis has been discussed in the following paragraphs.

The structure of the cathode $\text{CrO}_x\text{-B}$ after charge (de-lithiation) and discharge (lithiation) steps of first two cycles was analyzed using XRD. Since the pellet electrode has a different composition than that of the powder due to the addition of 10% carbon and 5% PTFE, it is necessary to know the difference in the diffraction patterns obtained for pellet electrode and the powder oxide sample. Fig. 3 shows the comparison of the X-ray diffraction patterns obtained for the powder and pellet samples of $\text{CrO}_x\text{-B}$. As expected, the XRD patterns for the pellet differed from that of the powder with additional peaks at several points. The reason

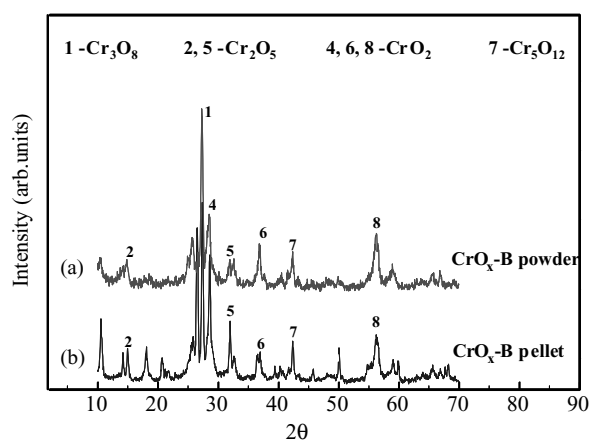


Fig. 3. XRD patterns for (a) powder and (b) pellet samples of $\text{CrO}_x\text{-B}$.

for this being the presence of carbon in the pellet sample which is more crystalline and hence all peaks are better visible in the pellet sample.

A charge step de-lithiates the sample and raises its voltage to 4.2 V at a rate of 0.5 mA/cm². A discharge step lithiates the sample with active Li⁺ ions and brings its voltage down to 2 V at the same rate. By identifying the various phases at the charged and discharged states, one could determine the causes for the irreversible losses occurring during galvanostatic cycling. This phase change would be complete within the first few cycles resulting in the formation of a reversible material and hence irreversible capacity losses would go to a minimum after the first few cycles. The fresh material itself is in the charged state and so the first cycle has only a discharge step in it. XRD analysis is done for four different CrO_x-B pellets at charged and discharged states of the first and second cycles. The first electrode pellet is a fresh sample, the second electrode pellet has undergone one discharge step, the third electrode pellet has undergone a discharge followed by a charge step and the fourth electrode pellet has undergone a discharge followed by a charge and discharge. X-ray diffraction is done on these four pellet electrodes and can be seen in Fig. 4 as patterns 'a', 'b', 'c' and 'd', respectively. The material remains as CrO_x in the charged state, whereas in the discharged state the material is Li_yCrO_x with the intercalation of *y* moles of Li⁺ ions. Approximately, 1.4 moles of Li⁺ participate in the intercalation [15].

During the first discharge step, a process of reduction or degradation of all the undesirable oxides takes place. As can be seen from the XRD patterns 'a' and 'b' in Fig. 4, the peaks for all the undesirable Cr₂O₅ and CrO₂, which are prominent in the fresh pellet, disappeared after first discharge. New peaks A and B have emerged in the discharged pellets that are results of structural changes of the active material due to lithium intercalation. The stoichiometry of the oxides corresponding to peaks A and B are not known. The pattern 'c' in Fig. 4 shows the XRD for the pellet in its second cycle charged state. The additional peaks A and B

that appeared after first discharge were not found in the second charged state and this confirms that there is a reversible structural change due to lithium insertion during discharge. The second discharge takes the pellet to the same form as it was in the first discharge state as seen from the XRD pattern 'd'. The material of the fresh pellet contains some unreacted CrO₃ and some impure oxides, which undergo irreversible reduction during the first discharge and then do not reappear anywhere and hence do not alter the reversibility of the material during further cycles. It is also worth noting that the peaks A and B that belong to the reduced state of CrO_x can be seen only in the discharged states (patterns 'b', 'd' and 'f'). The peaks corresponding to CrO₃ and some impure oxides seen in the pattern 'a' do not appear anymore after the first discharge, which indicates that all the impurities have undergone irreversible reduction. The charged and the discharged (patterns 'e' and 'f') state XRD patterns for the 10th cycle resemble that of the 2nd cycle, which indicate that after the 2nd cycle the material retains the same structure. This confirms that there is no further significant irreversible reaction taking place after the second cycle and only the reversible material takes part in the intercalation after the second cycle.

It is evident from the X-ray patterns that the material has attained a stable reversible structure for lithium intercalation after two cycles. All the irreversible oxides and other impurities have undergone reduction during the first discharge and become irreversible. The reduced impurities either stay inert or have undergone slow degradation during the course of cycling. The reduction process in the first discharge made the impurities amorphous and they cannot be seen in the XRD patterns after the first cycle.

3.4. Cycling performance of the new cathode material

Capacity fade is one of the major problems in all types of cathode materials for Li-ion cells. The capacity loss of cathode materials is caused by various mechanisms that depend on the cycling and storage conditions of the Li-ion cell. In general, capacity fade could be attributed to undesired side reactions that occur during overcharge or overdischarge, which causes electrolyte decomposition, passive film formation, active material dissolution and other phenomena, such as self-discharge and phase changes with continuous cycling.

Fig. 5 shows the comparison of galvanostatic charge–discharge curves for CrO_x-A and CrO_x-B at various cycles. The applied current density for lithiation (discharge) and de-lithiation (charge) is 0.5 mA/cm² and the cells were cycled between 2.0 and 4.2 V versus Li/Li⁺. Comparing the discharge characteristics of CrO_x-A and CrO_x-B after 20 and 100 cycles, the voltage plateau looks similar for both samples, but the specific capacity of CrO_x-B remained always higher than that of CrO_x-A for all cycles.

Fig. 6 shows the variation of lithiation capacity of both the samples with cycle number. Both samples exhibit an irreversible capacity loss of around 20 mAh/g. With contin-

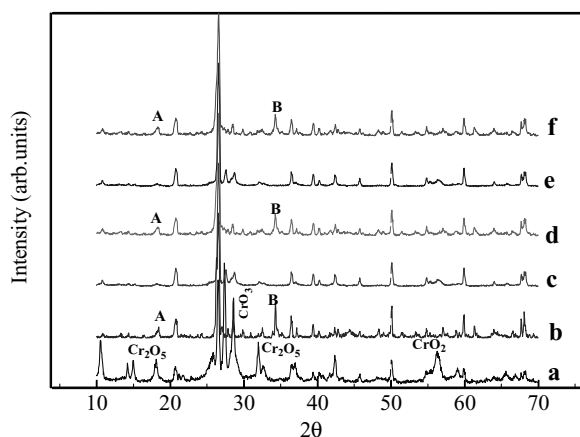


Fig. 4. XRD patterns of CrO_x-B sample at different stages: (a) fresh (1st charge); (b) 1st discharge; (c) 2nd charge; (d) 2nd discharge; (e) 10th charge; (f) 10th discharge.

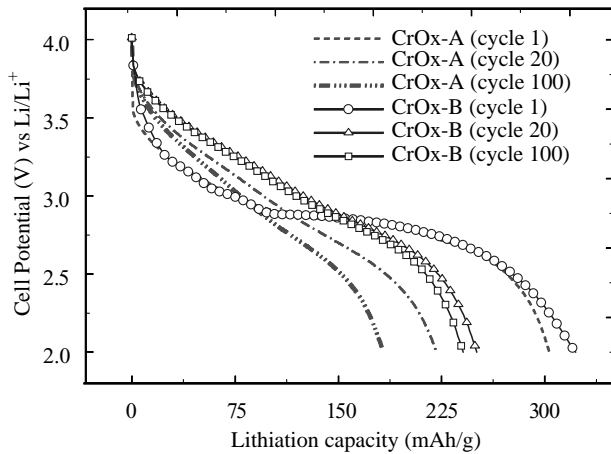


Fig. 5. Discharge profiles of $\text{CrO}_x\text{-B}$ and $\text{CrO}_x\text{-A}$ at 1, 20 and 100 cycles.

uous cycling, the lithiation capacity became almost stable for $\text{CrO}_x\text{-B}$ and it loses only an additional 19 mAh/g at the end of 100 cycles. In contrast, $\text{CrO}_x\text{-A}$ sample continues to lose its lithiation capacity with prolonged cycling and loses 51 mAh/g capacity between 2nd and 100th cycle.

Loss in capacity of the chromium oxide cathode material with cycling can arise due to formation of either surface layers or conversion of active material to inactive form. Thus, XRD material characterization was done on the electrode samples after various cycles. Fig. 7 presents the XRD analysis of the lithiated $\text{CrO}_x\text{-B}$ samples that were cycled 1, 20 and 100 times versus Li/Li^+ in their lithiated states. The XRD patterns after 100 cycles (Fig. 7) is similar to the patterns observed after 2nd and 20th cycles but the intensity of the peaks has reduced considerably. Moreover, the peaks for CrO_x and CrO_2 are blunt and broader after 100 cycles and the width of the peak measured at the half peak intensity has almost doubled when compared with the patterns obtained in 1st and 20th cycles. Peak intensity is decreased because of the disruption of the stable structure formed during lithiation step. As a result, lithium intercalation is affected due to

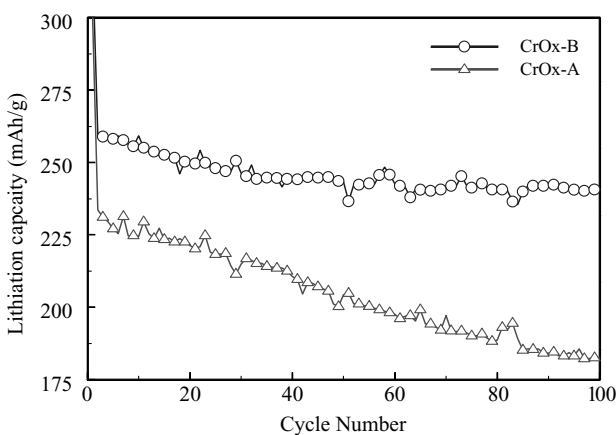


Fig. 6. Discharge capacities as a function of cycle number showing the capacity fade of $\text{CrO}_x\text{-A}$ and $\text{CrO}_x\text{-B}$ during cycling.

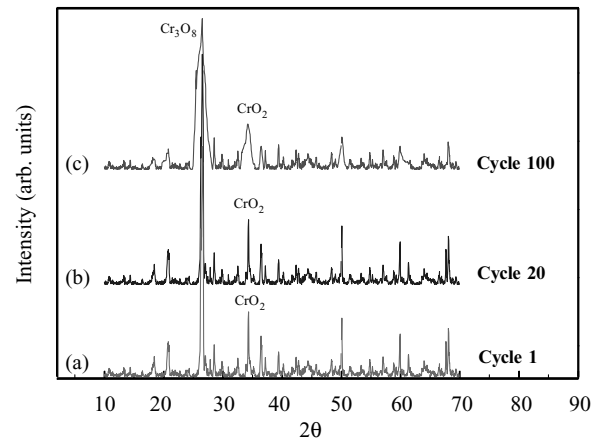


Fig. 7. XRD patterns of $\text{CrO}_x\text{-B}$ after (a) 1st cycle, (b) 20th cycle and (c) 100th cycle in lithiated state.

poor lithium diffusion coefficient and continuous growth of strong SEI layer. Aurbach et al. has reported similar observations, for $\text{Li}_x\text{Mn}_2\text{O}_4$ spinel oxides [16]. The morphological change is also analyzed by scanning electron microscopy (SEM) and has been discussed later on in the paper.

3.5. Impedance studies

One of the major factors that attribute to the capacity fade and a huge drop in cell potential during discharge is the impedance rise in the materials during prolonged cycling. Electrochemical impedance spectroscopy serve as an excellent tool for in situ characterization of the properties of insertion electrodes and the impedance characteristics can provide useful information on the stabilization and failure mechanisms of lithiated CrO_x electrode. The electrochemical impedance spectroscopy studies were done for $\text{CrO}_x\text{-B}$ at the end of 1st, 20th and 100th cycles. Fig. 8 shows the Nyquist plots of the fresh and cycled $\text{CrO}_x\text{-B}$ samples in completely de-lithiated state in the frequency range 10 mHz to 10 kHz.

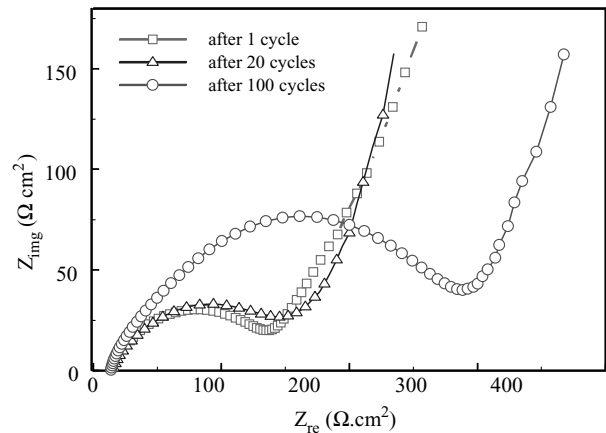


Fig. 8. Nyquist plots for $\text{CrO}_x\text{-B}$ in the frequency range 10 mHz to 10 kHz showing the variation of impedance of these electrodes during cycling.

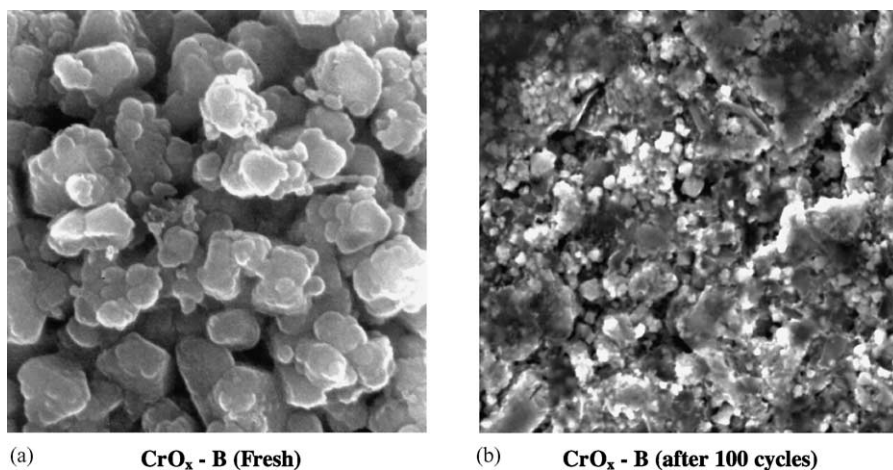


Fig. 9. SEM pictures of $\text{CrO}_x\text{-B}$: (a) fresh sample; (b) after 100th cycle.

The total impedance is the sum of the resistances of the electrolyte, surface film, charge transfer and diffusion. In general, Li-ion insertion into CrO_x is a series of multi-step process that involves migration of Li ions through the surface films covering the electrodes, followed by intercalation into the electrode material that involves charge transfer at the film–electrode interface which is then followed by solid state diffusion of lithium into the bulk of the host material. It can be seen from Fig. 8 that the total resistance of the electrode increases as a result of cycling. The reason for the impedance rise may be attributed to the increase in the resistance of the surface film and sluggish charge transfer kinetics as a result of cycling [17].

3.6. SEM studies

In order to analyze the changes in the surface morphology of the cathode after cycling, scanning electron micrographs were obtained for both fresh as well as cycled $\text{CrO}_x\text{-B}$ samples. Fig. 9 presents the SEM at a magnification of $20,000\times$, in which one could observe that the material has undergone a severe deterioration in its morphology with large number of cracks and pores that indicates rapid intercalation and deintercalation of Li^+ ions from the matrix. They also indicate heavy stress and volume expansion of the material due to prolonged cycling. The morphological and structural changes occurring in the cathode material with cycling can be classified into two types—those occurring during normal insertion–de-insertion of lithium and those occurring during overcharge conditions. This distortion in the surface morphology of the cathode may lead to poor diffusion of lithium into the bulk electrode material and this causes higher capacity loss with cycling. Lithium insertion in CrO_x involves major degradation of the intercalation host and after prolonged cycling, insertion of even small amounts of lithium leads to irreversible structural breakdown [15]. If discharged only up to 2 V, the surface morphological characteristics are retained during the first discharge, but a phase change de-

velops gradually during charging for this type of material [18].

3.7. Conclusion

Chromium oxide cathode materials are promising cathode materials for rechargeable lithium batteries. A new type of chromium cathode material $\text{CrO}_x\text{-B}$ is identified to have the best performance among the group of various different chromium oxides. Although amorphous Cr_3O_8 is believed to be the suitable cathode material, our results show that the crystalline Cr_3O_8 also behaves well as a cathode material. The stoichiometry of the new material is Cr_3O_8 and by optimizing the synthesis conditions and increasing the duration of thermal decomposition to 48 h, the newly developed $\text{CrO}_x\text{-B}$ is able to perform better than the m-CrO_x developed by Arora et. al. [11], in terms of initial capacity and capacity fade during cycling. The reasons for the irreversible capacity loss occurring in the chromium oxide materials are explained using XRD studies. The capacity fade phenomena of CrO_x are analyzed using the XRD, EIS and SEM studies. The capacity of $\text{CrO}_x\text{-B}$ is 240 mAh/g even after 100 cycles, which is much higher than any other commercially, used cathode material. Attempts have been made for better understanding of the chromium oxide cathode materials. The effect of electrolyte and temperature over the performance of these materials are yet to be analyzed and would be a useful area of research. Although the mechanisms of the electrode side reactions are very complex and have not been analyzed by anyone until now, there is a great scope for new developments in this area.

Acknowledgements

Financial support provided by National Reconnaissance Office for Hybrid Advanced Power Sources # NRO-00-C-1034 is acknowledged gratefully.

References

- [1] J. Desilvestro, O. Haas, *J. Electrochem. Soc.* 137 (1990) 5C.
- [2] H. Lauckand, S.C. Nijhawan, *Prog. Batteries Solar Cells* 5 (1984) 61.
- [3] Y. Toyoguchi, J. Yamamura, T. Matsui, J. Iijima, *The Electrochemical Society Extended Abstracts*, vol. 87-2, Honolulu, HI, 18–23 October 1987, p. 109 (Abstract 73).
- [4] D. Linden (Ed.), *Handbook of Batteries and Fuel Cells*, McGraw-Hill, New York, 1984, p. 11.
- [5] R.S. Schwartz, I. Fankuchen, R. Ward, Abstract of thesis submitted by Schwartz to Polytechnic Institute of Brooklyn, 1952, 1676 pp.
- [6] J.O. Besenhard, M. Schwake, N. Misailidis, *J. Power Sources* 26 (1989) 409.
- [7] Y. Takeda, R. Kanno, Y. Tsuji, O. Yamamoto, *J. Power Sources* 9 (1983) 325.
- [8] O. Yamamoto, Y. Takeda, R. Kanno, Y. Oyabe, *J. Power Sources* 20 (1987) 151.
- [9] R. Koksang, D. Fauteux, P. Norby, K.A. Nielsen, *J. Electrochem. Soc.* 136 (3) (1989) 598.
- [10] R. Koksang, S. Yde-Anderson, K. West, B. Zachau-Christiansen, S. Skaarup, *Solid State Ionics* 28–30 (1988) 868.
- [11] P. Arora, D. Zhang, B.N. Popov, R.E. White, *Electrochem. Solid State Lett.* 1 (6) (1998) 249.
- [12] D. Zhang, B.N. Popov, Y.M. Podrazhansky, P. Arora, R.E. White, *J. Power Sources* 83 (1999) 121.
- [13] B.N. Popov, D. Zhang, P. Arora, R.E. White, *Electrochem. Soc. Proc.* 98–16 (1998) 339.
- [14] K.A. Wilhelmi, *Acta Chem. Scand.* 22 (1969) 2565.
- [15] R. Koksang, P. Norby, *Electrochim. Acta* 36 (1) (1991) 127.
- [16] D. Aurbach, et al., *J. Power Sources* 81–82 (1999) 472.
- [17] D. Aurbach, et al., *Electrochim. Acta* 47 (27) (2002) 4279–4417.
- [18] J.O. Besenhard, R. Schollhorn, *J. Electrochem. Soc.* 124 (7) (1977) 968.